

Broadband (ULF-VLF) surface impedance measurements using MIMDAS.

Stephen J. Garner¹ David V. Thiel²

Key Words: Magnetotellurics, MIMDAS, surface impedance, telluric profiling, ULF, VLF

ABSTRACT

Electromagnetic radiation from distant, discrete, ground-to-cloud lightning return-strokes can be recorded as atmospherics (spherics), using both electric and magnetic field antennas. The Earth-ionosphere waveguide filters this radiation into the ULF-VLF radio bands from 3 Hz to 30 kHz with a notch centred at approximately 2 kHz. The relationship between the orthogonal horizontal electric and magnetic field signatures at the receiver is directly related to the surface impedance of the Earth at that point. Transforming the transient fields to the frequency domain allows the calculation of the surface impedance over the frequency range determined by the sample rate and record length. From this, resistivity versus depth models of the Earth can be determined. This paper demonstrates that a discrete spheric can be considered as a broadband vertically polarised plane-wave source suitable for magnetotelluric (MT) style geophysical surveying, and that the data collected could be used to deduce the near-surface resistivity profile. The results from measurements made with MIM Exploration's proprietary distributed acquisition system (MIMDAS) are presented. Multi-station data were acquired in a telluric profiling mode (without a magnetic field reference) to demonstrate spatial coherence and correlation with conventional MIMDAS MT pseudosections and IP inversion models. The advantages of the technique include the broad band of measurement and rapid data-acquisition time for reliable statistics. Valid data were collected between 24 kHz and less than 200 Hz and while stacking improves data integrity, useful information may be extracted from less than 5 ms of a 6 s record, corresponding to a single strong spheric. This technique has potential value in near-surface geotechnical applications and as an aid in removing statics from conventional continuous-MT survey data.

INTRODUCTION

Tickhonov (1950) and Cagniard (1953) suggested the measurement of the horizontal electric and magnetic field components from a distant radio source as a geophysical tool for subsurface mapping. This became the basis for magnetotelluric

(MT) and hybrid methods which take advantage of the natural signals from 1 kHz down to 10^{-5} Hz (Morrison and Nichols, 1997; Vozoff, 1991). However, it is well known that spherics have energy from the ultra-low frequency (ULF) into the very-low frequency (VLF) bands (Chapman and Matthews, 1953; Jöhler and Lilley, 1961). There is little energy around 2 kHz due to a change in propagation mode. While ambient background energy has been used routinely (Labson et al., 1985; Strangway et al., 1973), it is shown here that discrete spherics can be used to significantly higher frequencies for VLF-MT geophysical investigations (Garner and Thiel, 1996; Garner, 1998; Thiel et al., 1988, 1996). This technique is an alternative to artificial or controlled source techniques such as VLF and controlled source audio-magnetotellurics (CSAMT). There are cost and time savings inherent in collecting higher frequency information concurrently with a MIMDAS MT/induced polarisation (IP) survey, via VLF-MT, as opposed to a separate contractor conducted CSAMT survey. In addition, VLF-MT will not be affected by the possible geometrical (near-field effects) and logistical problems associated with the remote CSAMT transmitter and motor generator. Further, VLF-MT could replace portable single-frequency VLF techniques which have an uncertain future as they utilise the large navigation transmitters that are facing redundancy and risk being decommissioned due to advances in Global Positioning Systems (GPS).

THEORY

The configuration of the electromagnetic (EM) field above the surface is slightly different for sub-ultra-low frequency (ULF) pulsations than for spherics at higher frequency. The latter propagate horizontally (vertically polarised, grazing incidence) while the former are assumed to propagate vertically (horizontal or normal incidence). Both types of signal behave in the same way at and beneath the surface because of the very large resistivity contrast between the air and the Earth (Madden and Nelson, 1964). In the case of vertically polarised signals, such as VLF or spherics, the primary electric field just above the surface is nearly vertical and the associated primary magnetic field (H_y) is horizontal, transverse to the direction of propagation. If the Earth has finite conductivity, some of the transmitted signal penetrates the surface diffusing downward within (at most) $1-2^\circ$ of vertical. The Earth rapidly absorbs the energy and the induced telluric currents convert it to heat through ohmic losses. The leakage into the surface means that the Poynting vector must have a small real component vertically down, which forces the electric field to have a relatively small horizontal component (E_x) in the direction of propagation. Hence, the total electric field vector at the surface has a slight forward tilt in the direction of propagation. The E_x component is dependent on the ground conductivity and has different phase (ϕ) to the primary signal. Generally speaking the greater the resistivity of the ground, the greater the horizontal component of the E-field that drives the telluric currents. The fields are assumed uniform enough that they behave like plane waves above and within the Earth. For simple interpretation, one can assume that the source lies in the far field, and the radiation is a vertically polarised plane wave (Vozoff, 1991).

¹ MIM Exploration
2/55 Little Edward St
Spring Hill
Qld 4000
Phone: (07) 3214 9139
Facsimile: (07) 3214 9122
E-mail: sjgarner@bigpond.com

² School of Microelectronic Engineering
Griffith University
Nathan
Qld 4111
Phone: (07) 3875 7192
Facsimile: (07) 3874 5198
E-mail: d.thiel@me.gu.edu.au

The surface impedance (Z_s) is the ratio of the horizontal E-field component to the primary horizontal H-field component (Wait, 1970; Thiel, 1986),

$$Z_s = \frac{E_x}{H_y} \tag{1}$$

In the case of a uniform half space the surface impedance Z_s is directly related to the resistivity (ρ) of the medium and is equal to the intrinsic impedance (Z) (Neff, 1981) where,

$$Z = \sqrt{\frac{j\omega\mu}{\sigma + j\omega\epsilon}} \tag{2}$$

Here ω is angular frequency, μ is the magnetic permeability, ϵ the electric permittivity or dielectric constant and σ is conductivity in siemens/metre, which is the inverse of resistivity in ohm-metres given by

$$\rho = \frac{|Z_s|^2}{\omega\mu} \tag{3}$$

The argument of Z_s is phase (ϕ). In a uniform half space E_x leads H_y in ϕ by 45° and ρ is equal for all frequencies.

For the frequency bands of interest in this work, one can make use of the concept known as skin depth. Skin depth (δ) is the depth in metres that the signal penetrates into the medium before it is attenuated to $1/e$ of its value at the surface. Skin depth is given by

$$\delta \approx \sqrt{\frac{2}{\omega\mu\sigma}} \approx \frac{1}{\sqrt{\pi\mu\sigma f}} \approx 500\sqrt{\frac{\rho}{f}} \tag{4}$$

where $f = \omega/2\pi$ is the frequency of the incident radiation in Hertz.

In the two-layer case, some energy is reflected at the subsurface boundary affecting the surface impedance. In this case Z_s is equal to the intrinsic impedance of the top layer multiplied by a factor Q , given by the expression (Wait, 1970),

$$Z_s = \frac{E_x}{H_y} = QZ_1 \tag{5}$$

where Z_1 is the intrinsic impedance of the upper layer and Q is related to the intrinsic impedance of the two layers (Z_1 and Z_2) and the depth to the second layer (h_1) in metres. The factor Q can be calculated iteratively for additional layers and is given by

$$Q \approx \frac{Z_2 + Z_1 \tanh(\gamma_1 h_1)}{Z_1 + Z_2 \tanh(\gamma_1 h_1)} \tag{6}$$

where γ_1 is the propagation coefficient of the first layer.

The apparent resistivity in ohm-metres is given by

$$\rho_a = \frac{|Z_s|^2}{\omega\mu_0} \tag{7}$$

When the resistivity of the top layer is greater than that of the second layer ($\rho_1 > \rho_2$) ϕ is greater than 45° . When the resistivity of the top layer is less than that of the second layer ($\rho_1 < \rho_2$) ϕ is less than 45° . That is, for a two-layer model, the phase is asymptotic to 45° at both high and low frequency for a finite number of uniform layers. The apparent resistivity asymptotes to the bottom layer resistivity at low frequencies and to the top layer at high frequencies. When the depth to the second layer exceeds the skin depth in the top layer ρ_a approaches ρ_1 , that is the ground appears

to be a uniform half space. Further details of surface impedance theory can be found in McNeill and Labson (1991), Vozoff (1991) and Thiel (1988).

The telluric profiling method (Sheriff, 1994) involves measuring two or more electric field dipoles and calculating the amplitude ratio and phase difference. This is also known as in-line tellurics or electric field ratio tellurics. This technique is a hybrid of the telluric current method (Berdichevskiy, 1965) and is generally used as a reconnaissance method. Telluric profiling is a convenient method of obtaining useful VLF-MT information using distributed acquisition or multiple channel systems in the absence of magnetometers with sufficient bandwidth. In this method, the telluric data must be normalised or referenced to at least one in-line telluric (E_x) dipole.

Here, as is the practice for continuous MT profiling (Morrison and Nichols, 1997), H_y is considered to have little variation over a two-dimensional (2D) earth. Consequently, the following relationships are established from equation (1) for scalar telluric profiling,

$$Z_k = \frac{E_k}{H}, \quad Z_{ref} = \frac{E_{ref}}{H} \tag{8}$$

where the subscript k represents successive in-line E_x dipoles, the subscript 'ref' is assigned to the E_x reference dipole and H is a simplified representation of H_y . The telluric ratio then is given by

$$R_k = \frac{Z_k}{Z_{ref}} = \frac{E_k}{E_{ref}} \tag{9}$$

From the definition of apparent resistivity in equation 7, one can derive the following relationship

$$|R_k|^2 = \frac{\rho_{ak}}{\rho_{aref}} = \frac{|Z_k|^2}{|Z_{ref}|^2} = \frac{|E_k|^2}{|E_{ref}|^2} \tag{10}$$

which reduces to the following expression for the apparent resistivity of an arbitrary in-line dipole

$$\rho_{ak} = \rho_{aref} \left(\frac{|E_k|}{|E_{ref}|} \right)^2 = \rho_{aref} |R_k|^2 \tag{11}$$

and

$$\phi_k = \tan^{-1} \left(\frac{\text{Real}(R_k)}{\text{Imaginary}(R_k)} \right) \tag{12}$$

where ϕ_k is the phase of the telluric ratio of an arbitrary in-line dipole.

When the electrical conditions of the Earth beneath an arbitrary in-line dipole E_k are identical to those beneath the reference E_{ref} , $|R_k|=1$ and $\phi_k=0^\circ$. Ideally, the reference dipole would be located over a halfspace so that the signals recorded are the closest representation of the primary signal. A highly conductive top layer could, for all intents and purposes, be a half space for the frequency band of interest. In this case, simply adding 45° to ϕ_k may compare reasonably to the primary signal phase and the ρ_{aref} parameter in equation (11) becomes the resistivity of the half space. Alternatively, each dipole could be referenced against one or both of its neighbouring dipoles, or a vertical antenna could be used as an input reference. The second option has the advantage of measuring an element of the primary signal providing a means of accurately estimating VLF-MT phase.

INSTRUMENTATION AND DATA ACQUISITION

The initial experiments demonstrating the feasibility of using discrete spherics for surface impedance measurements through repeatable single-station measurements (Garner, 1998; Garner and Thiel, 1996; Thiel et al., 1996) utilised off-the-shelf analogue recording equipment in the field, with an analogue to digital setup in the laboratory. Ongoing experiments (Garner, 1998) are being conducted using MIMDAS, which is a broad-band, high-resolution, distributed (multi-channel) acquisition system. MIMDAS is designed to acquire networked multi-channel electrical and EM geophysical data, though it could be used to acquire seismic data. Each channel or data acquisition unit (DAU) is networked in series with a computer-interfaced central recording unit (CRU) and is capable of capturing 250,000 samples or 1 Mb of data at many hardware specific, but software selectable, sample rates. MIMDAS has four gain settings and is capable of 24-bit resolution at sample rates up to 4,800 samples per second (sps) and 19-bit resolution from 4,800 sps to 48 ksp/s inclusive.

MIMDAS MT is conducted in a manner similar to the continuous MT profiling method described by Morrison and Nichols (1997). The magnetic field is often measured at only one station on a network spread, as it is assumed relatively constant compared with the highly variable horizontal electric field. Figure 1 is a schematic of a 2 km MIMDAS MT network spread or layout. Here the vehicle-mounted CRU and computer are at the centre of the layout between 7400N and 7500N. Most of the DAUs, which are identified by a unique serial number, are coincident with an electrode and measure the potential of a 100 m in-line (E_x) dipole. DAUs 86 and 102 measure from magnetometers H_y and H_x respectively, all located at 7100N. DAU 85 measures an E_y dipole that is located at the magnetometer site.

During this work, an entire 2.8 km survey line was read in one layout with one set of orthogonal, horizontal magnetometers and a coincident E_y dipole at the centre of the line. The magnetometers used on this survey did not have sufficient bandwidth to capitalise on much of the information stored in the 48 ksp/s records. Consequently, surface impedance (telluric profile) transfer functions were calculated by referencing (normalising) the in-line (E_x) electric field dipoles with an E_x dipole at the end of the line.

Acquisition time was constrained by the large amount of data generated at high sampling rates (48 ksp/s). An event collected for 5.13 s (approximately 250,000 19-bit samples stored in 32-bit

words) amounts to 1 Mb of data per channel. Typically, on every survey line up to six 48 ksp/s events were collected on up to 32 channels (depending on line length) with an electrode spacing of 100 m ($a=100$). This can equate to 32 Mb per 5.13 s event or up to 192 Mb of raw 48 ksp/s data alone per line.

SIGNAL, DATA DISCRIMINATION AND PROCESSING

Spherics manifest as a burst of signal with power ranging from 1 Hz to more than 20 kHz and lasting several milliseconds. In previous studies, spheric waveforms have been classified into an initial high frequency oscillatory portion with maximum spectral power in the 4-10 kHz range, followed by a slow tail with most power below about 1 kHz. These spectral peaks shift apart and diminish in amplitude with increasing distance from the transmitter (Chapman and Matthews, 1953). Figures 2 and 3 are examples of spheric signatures acquired using MIMDAS. Figure 2 shows the entire time series and a close up of a 48 ksp/s event for one channel (DAU 78) measuring electric field (E_x). Figure 3 shows the same spheric in a 256-sample time series for a number of channels demonstrating strong coherence from one channel to the next. Figure 4 displays the electric field power spectra on a log-log scale for the same DAUs as depicted in Figure 3. In this case, the dead band is evident between 1 kHz and 5 kHz. Note for Figures 3 and 4 that the DAUs are not necessarily ordered in-line by serial number.

Thiel et al. (1988) reported that when using the 4 kHz instrument an average of 15 suitable spherics were detected over a period of roughly 20 minutes. During one day there may be as many as 200-300 spherics received that are suitable for processing. During MIMDAS surveys it has been observed that the number of spherics in a 20 minute period may vary from less than 100 to 1000 depending on the time of day and time of year. Indeed, the upper estimate may be conservative when considering the number of spherics present in some 5.13 s events sampled at 48 ksp/s, such as shown in Figure 2. Qualitative observations of the time-series data indicated that the majority of spheric events were complete within 5 to 10 ms. For this work, an FFT length or spheric window of 256 samples was used (incorporating a 50 point pre-trigger), which resulted in 128 frequencies below 24 kHz, with a resolution of 187.5 Hz.

Two reference channels for each 5.13 s event were scanned for valid spherics and compared to ensure that the spherics identified correspond in time. The scanning process involved determining the

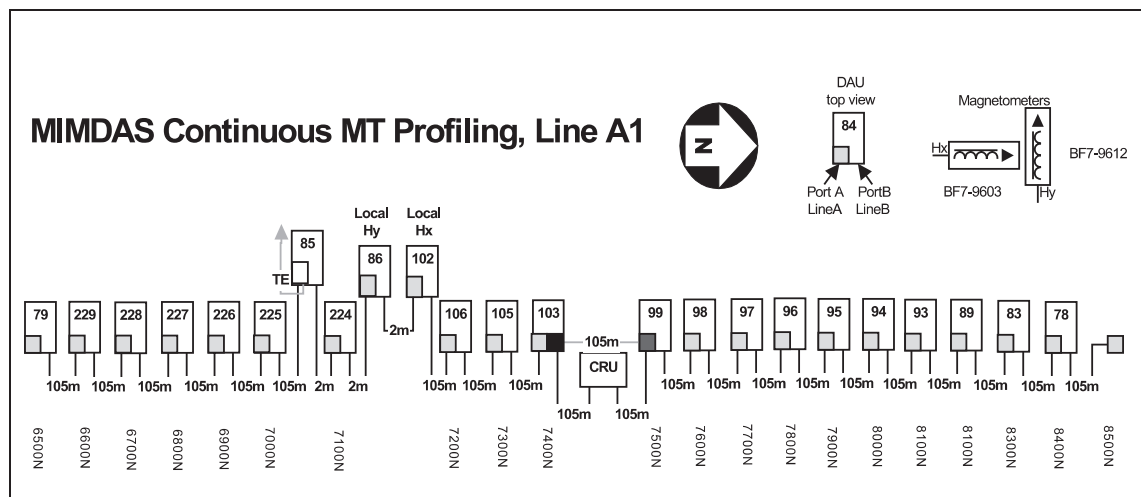


Fig. 1. A layout diagram representing a MIMDAS magnetotellurics survey line. This shows the position of networked data acquisition units (DAUs) and the central recording unit (CRU). Each DAU is labelled with a unique serial number and measures a 100 m dipole, with the exception of 86 and 102 that measure from the H_y and H_x magnetometers respectively.

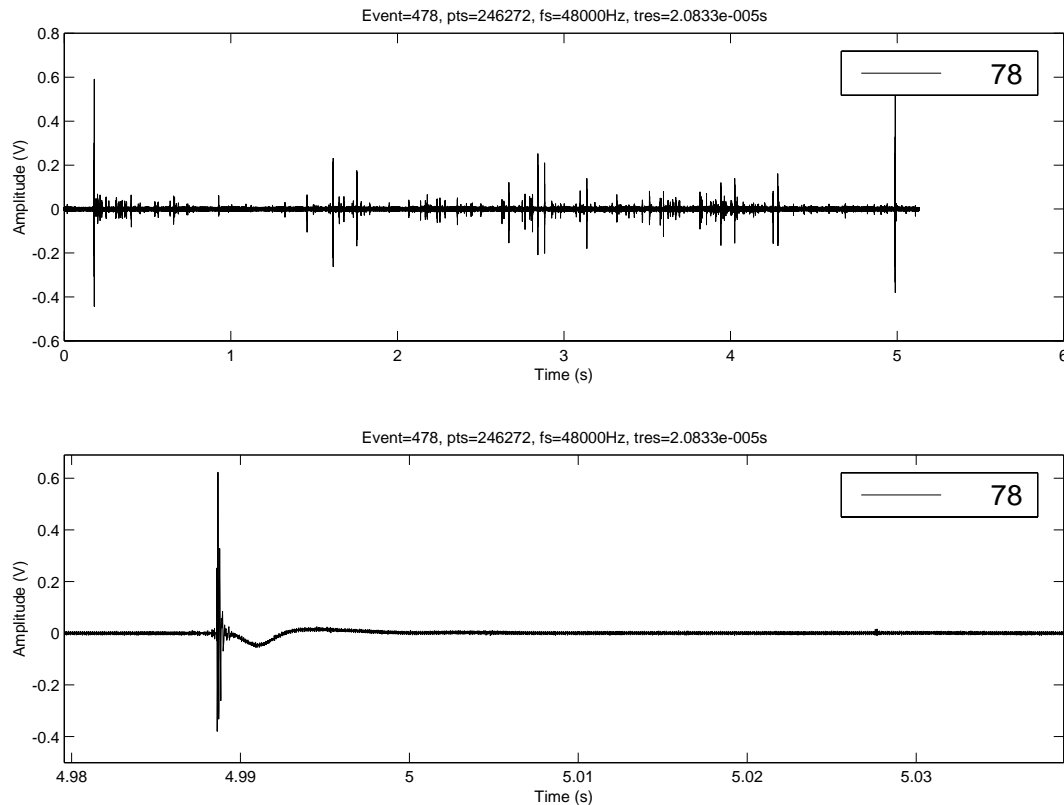


Fig. 2. An electric-field (E_x) time-series sampled at 48 ksp/s using MIMDAS (DAU 78). The top panel exhibits the entire event, while the lower panel depicts a close-up view of an individual spheric from that event. The sample rate and resolution in time are denoted by fs and $tres$, respectively.

mean and standard deviation and then finding excursions of three standard deviations or more in the amplitude of consecutive samples. When a spheric was detected coincidentally on both reference channels the index was stored in a master file and then advanced to the start of the next potential spheric window. The data corresponding to these discrete spherics were then transformed to the frequency domain using these indices as a trigger point. Transfer function estimates were calculated using ordinary stochastic methods, with and without outlier rejection. The outliers were discarded by keeping the best 80% of the normal distribution for each frequency 'bin', before further stacking.

RESULTS

Multi-layer modelling was conducted using parameters commonly encountered by MIM geoscientists. When varying a top layer of 5-10 Ωm in thickness from 1-90 m, it was found that much of the signal in the 200 Hz to 20 kHz band would be unlikely to penetrate significant conductive cover (10 m or more). It is clear from this kind of simple analysis that surface impedance information in the frequency band 200 Hz to 20 kHz can provide useful information about thin, near-surface conductive or resistive zones. These localised features give rise to static shifts (statics) that can significantly distort the pseudosections and affect the interpretation of MT surveys (Morrison and Nichols, 1997). To supplement conventional MIMDAS IP and MT data, the higher frequency VLF-MT data are often collected in order to detect features that give rise to statics and may otherwise be undetectable.

Figure 5 is a schematic representation of the expected geological cross section for a recent MIMDAS survey (Garner, 1998). For brevity, data for just one of eleven lines in the grid is presented. All lines in this area were oriented perpendicular to the strike of a banded iron formation (BIF) ridge that runs roughly

east-west while dipping steeply ($70\text{-}80^\circ$) to the south-southeast. The BIF and cherts outcrop at the top of the range. Massive pyrite lenses are known to exist over much of the strike length of the range, but are usually south of the BIF ridge. The northern slope and plain hosts a profile of conductive clays to roughly 80 m, overlain by a layer of massive hard-panned scree (caliche/calcrete) which in turn is covered by a thin layer of sandy soil. This hard pan layer, which is sporadically divided by palaeochannels, was only discovered when attempting to build satisfactory IP current and potential electrodes. The MIMDAS survey grid was planned to detect conductive targets corresponding to volcanic-hosted massive sulphide (VHMS) Fe-Cu-Zn mineralisation in the Archaean felsic volcanic package to the north of the range. In this case, no VHMS was detected.

A shallow, resistive, and chargeable zone, overlying a conductive feature dominates the inverted IP model sections in Figure 6. This is attributable to near-surface weathered regions of the BIF coinciding with the topographical high located between 7400-7500 m. The anomalous chargeability may be the signature of magnetite and haematite in the BIF, or an adjacent pyrite lens. The conductive cover to the north of the BIF ridge from 7700 m to 9400 m appears to be 50-100 m thick with resistivity of the order of 10-50 Ωm , consistent with previous DC-sounding results. The worst case for VLF-MT sounding is an effective depth penetration for 24 kHz and 187.5 Hz, ranging from roughly 10 m to 100 m respectively.

Figure 7 shows telluric-ratio sections for a single reference (E_{ref2}) located at the southern extreme of the survey line (6900 m). This also locates the reference's single colour reference stripe at the southern end of the pseudosection. The reference stripes in phase ϕ_k and amplitude $|R_k|$, equating to 0° and 1 respectively, correspond to the telluric ratio of the reference dipole with itself. Note that R_k

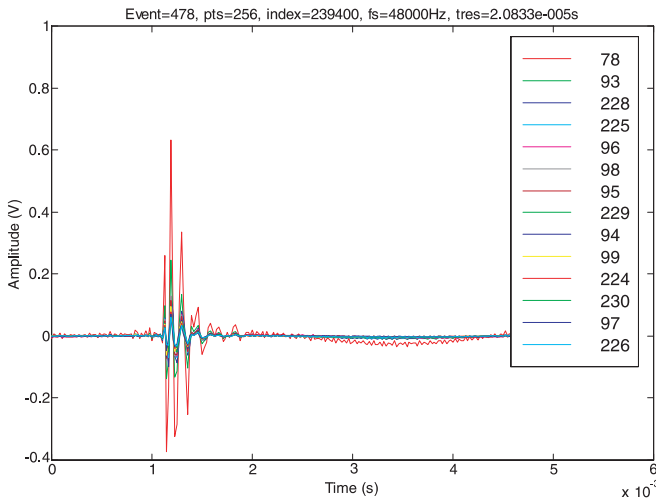


Fig. 3. A multi-channel, 256-sample (pts), close-up of a 48 kpsps (fs) time-series spheric from Figure 2. Each channel represents a uniquely numbered DAU. The index marks the start of the spheric in the full time series for event 478. The sample rate and resolution in time are denoted by fs and tres, respectively.

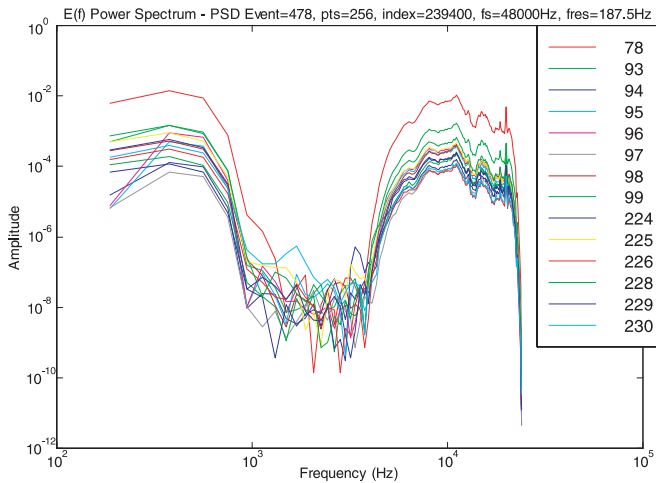


Fig. 4. A multi-channel electric-field power spectra of the spheric displayed in Figure 3. Each channel represents a uniquely numbered DAU. The index marks the start of the spheric in the full time series for event 478. The sample rate and resolution in frequency are denoted by fs and fres, respectively.

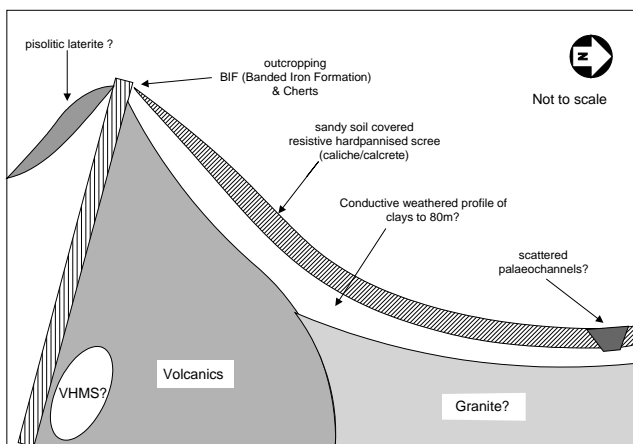


Fig. 5. Schematic geological section of the area around the banded iron formation ridge crossed by to the MIMDAS MT/IP survey line. The survey was planned to detect a possible VHMS deposit. The survey line extended from the flats to the south of the range for 2.8 km out onto the northern plains. This diagram is not drawn to scale.

is a dimensionless parameter derived from the ratio of two electric field dipoles. The BIF (7400 - 7500 m), is mapped as a resistive band at all frequencies in $|R_k|$ and a more subtle ϕ_k anomaly that varies with depth. The $|R_k|$ data also indicates a resistive shallow layer attributable to the hard pan on the plains to the north of the BIF range was beyond the resolution of the other techniques. The narrow conductive stripe in conjunction with the broader and deeper phase anomaly just south of 8000 m may correspond to the smaller, chargeability feature at around 8000 m. Regions of extremely high conductivity are evident in Figure 7 near 8800 m and 9400 m and may indicate palaeochannels. A slight perturbation is evident in both $|R_k|$ and ϕ_k at around 19.8 kHz corresponding to the North West Cape VLF transmitter. The dead band is evident as a region of noisier data between 1 kHz and 5 kHz.

While there is a noticeable variation in MT phase in Figure 8 corresponding to the BIF, it is evident at all frequencies in the MT apparent resistivity as highly resistive. This may be indicative of statics as this is only a relatively shallow resistive feature in the IP resistivity model of Figure 6.

DISCUSSION

This work demonstrates that discrete spherics can be used as a source for broad-band (187.5 Hz to 24 kHz) surface impedance measurements (VLF-MT). In the presence of strong signal, interpretable impedance information can be obtained from very short sampling intervals (less than 25 s) and possibly even a single discrete spheric.

The R_k data presented strongly suggests that VLF-MT is mapping near-surface inhomogeneity in the cover that is beyond the vertical resolution of both MT and IP as conducted for this work. These data demonstrate strong spatial correlation with lateral variation in known geology as well as the pseudosections or inversion models of conventional techniques. VLF-MT data can be used to help resolve structure in the near-surface resistivity allowing the delineation of shallow inhomogeneities that give rise to static shifts in conventional MT data. These data can be collected using MIMDAS during conventional MT surveys with little cost in time.

This technique would be valuable in high-resistivity environments and near-surface geotechnical and environmental

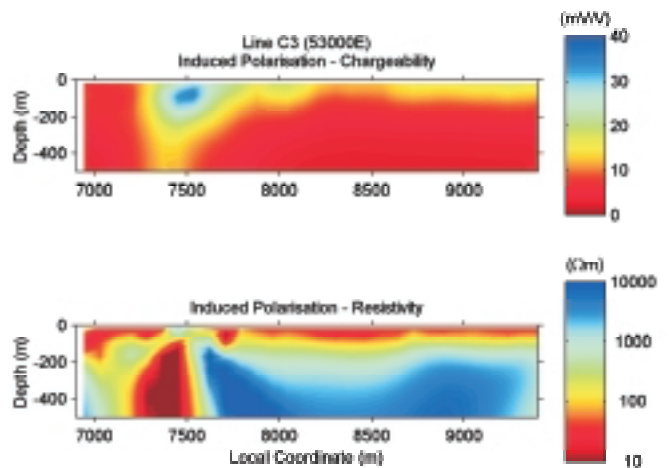


Fig. 6. The inverted data model sections of the MIMDAS induced polarisation (IP). The top and bottom panels are model sections produced from the inversion of IP chargeability and resistivity data respectively. The vertical scale is depth from the surface in metres and the horizontal scale is the local grid Northing.

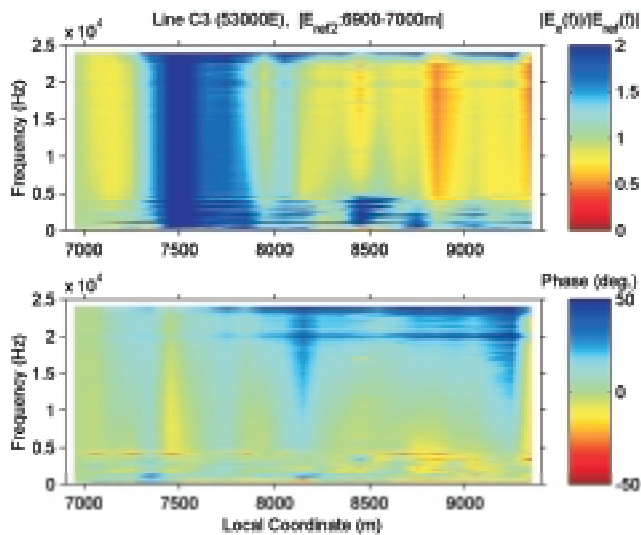


Fig. 7. A VLF-MT telluric profile (Eref2) pseudosection of data collected by MIMDAS from the same layout as used for Figure 6. The top and bottom panels represent telluric ratio amplitude versus frequency and phase versus frequency, respectively. The horizontal scale is the local grid Northing.

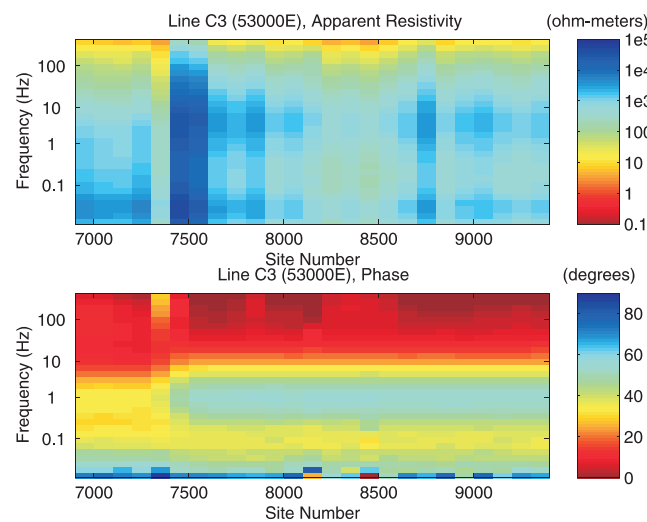


Fig. 8. The MIMDAS magnetotelluric (MT) pseudosection from the same survey line represented in Figures 6 and 7. The top and bottom panels represent apparent resistivity versus frequency and phase versus frequency, respectively. The horizontal scale is the local grid Northing.

applications, filling a niche between audio-magnetotellurics and ground penetrating radar. Ultimately, VLF-MT is competing against high-frequency controlled-source surface impedance techniques like CSAMT, without the geometrical (near field) and logistical problems associated with a portable artificial source. VLF-MT will provide an alternative to passive VLF in case of transmitter decommissioning.

ACKNOWLEDGEMENTS

The author acknowledges with gratitude MIM and joint venture partners for allowing the presentation of the data and John E. E. Kingman for training in the operation of MIMDAS and management of the data acquired. I would like to thank the various (anonymous) MIMEX geoscientists for their technical advice via personal communications and internal reports. Finally, I would like to acknowledge the various members of the MIMDAS field crews that have worked with me during the collection of data.

REFERENCES

- Berdichevskiy, M.N., 1965, Electrical prospecting with the telluric current method, Keller, G.V., Transl. and Ed.: Quarterly of the Colorado School of Mines, 60.
- Cagniard, L., 1953, Basic theory of the magnetotelluric method of geophysical prospecting: *Geophysics*, 18, 605-635.
- Chapman, F.W. and Matthews, W.D., 1953, Audio-frequency spectrum of atmospherics: *Nature*, 172, 495.
- Garner, S.J., 1998, Broadband surface impedance measurements using VLF spherics and artificial HF: Ph.D. thesis, Griffith University.
- Garner, S.J. and Thiel, D.V., 1996, Broad band VLF surface impedance measurements using atmospherics: *Eos Trans. AGU*, 77, No22, West. Pacif. Geophys. Meet. Suppl., W21.
- Garner, S.J., Thiel, D.V. and O'Keefe, S.G., 1997, Surface impedance time domain reflectometry for the determination of ice depth: *Geophys. Res. Lett.*, 24, 1599-1602.
- Johler, J.R. and Lilley, C.M., 1961, Ground-conductivity determinations at low frequencies by an analysis of spheric signatures of thunderstorms: *J. Geophys. Res.*, 66, 3233.
- Labson, V.F., Becker, A., Morrison, H.F. and Conti, U., 1985, Geophysical exploration with audiofrequency magnetic fields: *Geophysics*, 50, 656-664.
- Madden, T.R. and Nelson, P., 1964, On the relation between telluric currents and the earth's magnetic field, in Vozoff, K., Ed., *Magnetotelluric methods: SEG geophysics reprint series 5*, 89-102.
- McNeill, J.D. and Labson, V.F., 1991, Geological mapping using VLF radio fields: in Nabighian, M. N., Ed., *Electromagnetic methods in applied geophysics*, Soc. Expl. Geophys. 2B, 521-640.
- Morrison, H.F. and Nichols, E.A., 1997, Mineral Exploration with Natural Electromagnetic Fields: in Gubins, A.G., Ed., *Proc. Expl. 97: Fourth Decennial Internat. Conf. Min. Expl.*, 527-540.
- Neff, H.P.Jr., 1981, *Basic Electromagnetic Fields*: Harper and Row, Publishers, Inc.
- Sheriff, R.E., 1994, *Encyclopedic dictionary of exploration geophysics: Geophysical References Series 1*, Soc. Expl. Geophys.
- Strangway, D.W., Swift, C.M.Jr. and Holmer, R.C., 1973, The application of audio-frequency magnetotellurics (AMT) to mineral exploration, *Geophysics*, 38, 1159-1175.
- Thiel, D.V., 1986, A preliminary assessment of glacial ice profiling using VLF surface-impedance measurements: *J. Glaciol.*, 32, No112, 376.
- Thiel, D.V., 1988, VLF electromagnetic prospecting: in Finkl, C.W.Jr., Ed., *The encyclopedia of field and general geology*.
- Thiel, D.V., Garner, S.J. and O'Keefe, S.G., 1996, ELF surface impedance measurements for subsurface earth mapping using discrete spherics from distant lightning as a radiation source: *URSI conference*, January 1996.
- Thiel, D.V., Wilson, M.J. and Webb, C.J., 1988, A surface impedance mapping technique based on radiation from discrete lightning strokes: *Geoexpl.*, 25, 163.
- Tickonov, A.N., 1950, Determination of the electrical characteristics of deep strata of the earth's crust: *Dok. Akad. Nauk., USSR*, 73, 295-297.
- Vozoff, K., 1991, The magnetotelluric method: in Nabighian, M.N., Ed., *Electromagnetic methods in applied geophysics*, Soc. Expl. Geophys., 2B, 641-711.
- Wait, J.R., 1970, *Electromagnetic waves in stratified media: A Classic Reissue*, IEEE Press, 1996.